AMBIENT TO HIGH-TEMPERATURE FRACTURE TOUGHNESS AND CYCLIC FATIGUE BEHAVIOR IN ALCONTAINING SILICON CARBIDE CERAMICS

R. Yuan, J. J. Kruzic, X. F. Zhang, L. C. De Jonghe, and R. O. Ritchie

Materials Sciences Division, Lawrence Berkeley National Laboratory
and
Department of Materials Science and Engineering,
University of California, Berkeley, CA 94720, USA

Ambient to High-Temperature Fracture Toughness and Cyclic Fatigue Behavior in Al-Containing Silicon Carbide Ceramics

R. Yuan, J. J. Kruzic, X. F. Zhang, L. C. De Jonghe, and R. O. Ritchie

Materials Sciences Division, Lawrence Berkeley National Laboratory, and
Department of Materials Science and Engineering,
University of California, Berkeley, CA 94720, USA

Abstract—A series of *in situ* toughened, Al, B and C containing, silicon carbide ceramics (ABC-SiC) has been examined with Al contents varying from 3 to 7 wt%. With increasing Al additions, the grain morphology in the as-processed microstructures varied from elongated to bimodal to equiaxed, with a change in the nature of the grain-boundary film from amorphous to partially crystalline to fully crystalline. Fracture toughness and cyclic fatigue tests on these microstructures revealed that although the 7 wt.% Al containing material (7ABC) was extremely brittle, the 3 and particularly 5 wt.% Al materials (3ABC and 5ABC, respectively) displayed excellent crack-growth resistance at both ambient (25°C) and elevated (1300°C) temperatures. Indeed, no evidence of creep damage, in the form of grain-boundary cavitation, was seen at temperatures at 1300°C or below. The enhanced toughness of the higher Al-containing materials was associated with extensive crack bridging from both interlocking grains (in 3ABC) and uncracked ligaments (in 5ABC); in contrast, the 7ABC SiC showed no such bridging, concomitant with a marked reduction in the volume fraction of elongated grains. Mechanistically, cyclic fatigue-crack growth in 3ABC and 5ABC SiC involved the progressive degradation of such bridging ligaments in the crack wake, with the difference in the degree of elastic vs. frictional bridging affecting the slope, i.e., Paris law exponent, of the crack-growth curve.

Keywords: Ceramics; Structural SiC; Mechanical properties (fracture toughness, fatigue); Grain bridging; Uncracked ligaments

I. Introduction

Silicon carbide (SiC) ceramics represent a class of materials that may potentially replace Ni-base superalloys as higher temperature engine materials because of their high strength, low density and superior oxidation/creep resistance above 1100°C. However, one principal factor which limits their application is their low fracture toughness, which in commercial material is typically on the order of 2-3 MPa√m. In light of this, much recent research on SiC [1-11] has focused on ways to increase this toughness. Of these, the approach of *in situ* toughening with aluminum, boron and carbon additions to produce so-called ABC-SiC [3] has been particularly successful in increasing the ambient-temperature fracture toughness to above 9 MPa√m [7], which is the highest toughness ever reported for SiC. This was achieved in a 3 wt.% Al-containing material (3ABC-SiC) by developing a microstructure of interlocking, high aspect-ratio grains, separated by grain boundaries weakened by the presence of a thin intergranular glassy film; this in turn induced intergranular fracture and consequent extrinsic toughening[1] from the bridging of interlocking grains in the crack wake [7]. However, under cyclic loads, 3ABC-SiC was found to be susceptible to fatigue-crack growth, due to a cyclic-loading induced degradation in the zone of grain bridging in the crack wake [7,8].

Subsequent work on 3ABC-SiC at elevated temperatures [9-11,13] revealed that the fracture toughness and fatigue-crack growth properties were only marginally decreased at temperatures up to 1300°C, with no apparent change in cracking and shielding mechanisms; furthermore, little or no evidence of creep damage, in the form of grain-boundary cavitation, could be detected at temperatures below 1350°C [13]. This excellent combination of low-temperature toughness and high-temperature toughness/creep behavior was found to be the result of a remarkable property of 3ABC-SiC, that of the *in situ* crystallization of the intergranular glassy films at temperatures above ~1100°C [9-11,13,14]. Moreover, although the grain-boundary films remain

---

[1] *Extrinsic* toughening involves micro-mechanisms, such as crack bridging or microcracking, which act primarily in the crack wake to *locally* "shield" the crack from the applied (*global*) driving force; they therefore enhance the crack-growth toughness and invariably result in resistance-curve behavior. They are to be compared with *intrinsic* mechanisms which operate ahead of the crack tip to enhance the inherent toughness of the material; these mechanisms mainly promote resistance to crack initiation [12].

crystalline, the high toughness was retained, indeed increased, on subsequently cooling to room temperature [10].

Accordingly, from the prospective of developing SiC with such optimized properties, two means of controlling microstructures in ABC-SiC can be contemplated. The first of these is to anneal the material (e.g., at 1300˚C) prior to use to cause the crystallization of the amorphous grain-boundary films. Chen *et al.* [9-11] found that in addition to conferring good high-temperature creep and fatigue resistance, such heat treatments led to a ~20% increase in the room-temperature fracture toughness and fatigue-crack growth resistance (with no change in mechanism), compared to that in the as-hot-pressed material. However, an alternative approach is via microstructure modification through compositional changes, specifically by varying the aluminum content [15]. To date, several ABC-SiC materials have been processed with aluminum contents between 3 and 7 wt.%, where the changing Al additions resulted in significantly altered microstructures [7-11,15]. Whereas the 3 wt.% material (3ABC) develops a microstructure of relatively uniform elongated grains with amorphous grain-boundary films (as noted above), a bimodal distribution of both elongated and equiaxed grains with partially crystallized grain-boundary films is seen in the 5ABC material, compared to principally equiaxed grains with only a few elongated (needle-like) grains, all with fully crystallized grain boundaries, in the 7ABC-SiC.

The focus of the present work is to present a detailed examination of the fracture toughness and fatigue properties of three ABC-SiC microstructures at ambient to elevated temperatures (25° to 1300°C), with the objective of defining the salient damage and toughening mechanisms and their relationship to the characteristic microstructures involved.

II. Experimental Procedures

(1) Processing of ABC-SiC

Submicron β-SiC powder (Betarundum, Grade ultrafine, IBIDEN, Japan), with a mean particle size of 0.27 μm, was mixed with Al, B and C additives in toluene. The Al powder (H-3, Valimet, Stockton, CA), which had an average size of 3 μm, was added in amounts of 3, 5 and 7 wt.%, whereas the boron (Callery Chemical, Callery, PA) was kept

constant at 0.6 wt.%. The carbon was introduced as 4 wt.% Apiezon wax, which on pyrolysis yielded ~2 wt.% C content. The slurry was ultrasonically agitated, stir-dried and sieved through a 200 mesh screen. After cold die compression at 35 MPa, the green compacts were hot-pressed at 1900˚C for 1 h at 50 MPa pressure in graphite dies lined with graphite foil, under a constant gaseous argon flow at 7 kPa, to produce ~ 4 mm thick, 38 mm diameter disks. Unless noted, all results presented are from samples tested in the as-processed state; however, for a few room temperature experiments specimens were tested after ~ 72 h at 1300˚C in flowing argon, to see if prolonged exposure to elevated temperatures affects the room temperature properties.

(2) Microstructure Characterization

After diamond grinding ~500 μm off each surface, both sides of the hot-pressed pellets were polished to a 1 μm finish. Densities of the hot-pressed specimens were determined by Archimedes' method and found to be greater than 99% of theoretical density for all samples.

X-ray diffraction (XRD) was carried out on the polished surfaces of the disks over the range from 20˚ to 80˚ (2θ) at steps of 0.05˚, with a time constant of 1 s. Quantitative analysis of the SiC polytypes for each microstructure was carried out using the X-ray peak intensities by considering the four most common polytypes, 3C, 4H, 6H, and 15R, using the system of equations derived by Ruska *et al*; details of this method may be found in Ref. [16].

Grain morphology was observed using field-emission scanning electron microscopy (SEM) (secondary electron mode) of both polished and plasma etched specimens. High-resolution transmission electron microscopy (HRTEM) was performed to examine the nature of the grain boundaries using 3 mm diameter disks which were sliced from bulk SiC. After mechanical grinding and polishing down to 100 μm thick, the central area of each disk was dimpled to 10 μm thick, and then argon ion milled to make the samples electron transparent. Microstructural characterization was performed in a 200 kV field-emission-gun Philips CM200 transmission electron microscope, equipped with an energy-dispersive X-ray spectroscopy (EDS) system for chemical microanalysis.

(3) Fracture and Fatigue Testing

Resistance curves (R-curves) and fracture toughness K_c values were determined using fatigue precracked, 3 mm thick, disk-shaped compact-tension DC(T) samples (with a width of $W = 28$ mm), in general accordance with ASTM Standard E-399. The notch depth was ~ 9 mm (~0.3 W), such that crack sizes, a, after precracking were typically 11 to 17 mm in length. Precracking was performed at ambient temperature by cyclic fatigue loading the DC(T) specimens, which contained half-chevron notches; procedures are described in ref. [17]. Prior to R-curve testing, precracked specimens were additionally cycled for ~24 hr at a stress-intensity range just below the ΔK_{th} fatigue threshold in an attempt to minimize the presence of bridging ligaments in the crack wake; no further crack extension was detected by compliance techniques or optical microscopy during this period. For 7ABC samples, fatigue precracking was not possible due to the inherent brittleness of this microstructure. Accordingly, to get an upper bound for the toughness, fracture toughness tests were conducted using "razor micronotched" samples with a root radius of ~20 μm instead of an atomically sharp precrack. Micronotches were produced by repeatedly rubbing a razor blade over the tip of a straight saw-cut notch in the presence of a 1 μm diamond slurry.

At ambient temperatures, R-curves were determined to evaluate the toughness of the 3ABC and 5ABC microstructures; however at elevated temperatures, due to the difficulty of conducting such tests at 1300ºC, single-value fracture toughness values were obtained by computing K_c from the peak load at fracture using standard stress-intensity solutions [18]. Ambient-temperature tests were conducted in controlled room air (25°C, ~45% relative humidity), whereas all testing at higher temperatures was carried out in flowing argon gas at atmospheric pressure in an environmental chamber/furnace with graphite elements, which maintained the specified temperature to within ±1˚C.

Cyclic fatigue-crack growth testing was also performed at 25° and 1300°C in identical environments using similar-sized DC(T) specimens, in general accordance with ASTM Standard E-647, modified for brittle materials using procedures outlined in ref. [17]. Samples for testing at both low and high temperatures were initially fatigue precracked at ambient temperature, as described above. All testing was performed on computer-controlled MTS servo-hydraulic testing machines, operating at a test frequency of 25 Hz (sinusoidal waveform) and a tension-tension load ratio (ratio of minimum to maximum

loads) of $R = 0.1$. Fatigue-crack growth rates, da/dN, were determined under stress-intensity K control over five decades of growth rates from threshold to instability ($\sim 10^{-11}$ to 10^{-6} m/cycle). The ΔK_{th} and $K_{max,th}$ fatigue thresholds, which were operationally defined at minimum growth rate of 10^{-10}–10^{-11} m/cycle, were approached under decreasing K (load-shedding) conditions using a normalized K-gradient ($1/K.dK/da$) of 0.1 mm^{-1}.

For both toughness and fatigue-crack growth tests, crack lengths were monitored at ambient temperatures using back-face strain, elastic unloading compliance methods [19]. Measurements were made with a 350Ω strain gauge (1.92 mm gauge length), affixed to the center of the back face of the test samples, using the numerical compliance relationship between crack length and back-face strain for the DC(T) specimen taken from ref. [20]. Crack lengths were continuously monitored *in situ* and recorded at 25 μm increments; corresponding growth rates were computed by averaging over crack extensions of 100 μm.

Corresponding crack length measurements at elevated temperatures were carried out using a direct-current electrical-potential drop method [9,21], which was made possible by the fact that there is a significant decrease in electrical resistivity ρ of silicon carbide above 600˚C ($\rho \sim 10$ Ωm). This approach involves passing a constant current through the DC(T) specimen and measuring the potential developed across the notch, using a relationship between voltage and crack length determined both numerically and experimentally in Ref. [20] for the DC(T) geometry. A constant direct current of $\sim$400-800 mA was used so that the initial output potential was 0.4 V. Full details are given in refs. [9,21].

Due to crack bridging, errors were invariably incurred in the compliance and potential crack-length measurements; accordingly, verification of the crack length was achieved via optical microscopy. For elevated temperature tests, samples were periodically cooled down to ambient temperature to verify the crack size. Discrepancies between the compliance/electrical-potential and optically measured crack length were corrected by assuming that the error accumulated linearly with crack extension.

(4) Fractography

Fracture surfaces and corresponding crack paths for cracks grown under both monotonic and cyclic loads were examined in the SEM in the secondary electron mode. The crack paths were used to examine how the crack interacted with the salient features of the microstructure, and were obtained by metallographically polishing sections taken perpendicular to the crack surface. Additionally, the damage regions around the crack tip after fatigue cycling were examined using TEM, with specimens prepared as described above, using special care to ensure that the crack tips were in the thinnest, electron transparent, region.

(5) Crack-Opening Profile Measurements

To assess the differences in grain bridging, crack-opening profile measurements were made by *in situ* loading one 3ABC and one 5ABC sample with almost identical crack lengths in the field-emission SEM, after R-curve measurements had been made. Each sample was loaded to an applied driving force of 6.2 MPa m, corresponding to ~82% of the driving force need for crack extension in the 3ABC material (i.e., peak toughness). Measurements of the full crack opening, $2u$, were made at a resolution of 10 nm at magnifications of up to 30,000X near the crack tip. The crack lengths were also measured *in situ* to be sure crack extension did not occur during loading. Readings were made at ~50 μm increments to give an adequate number of data points to get a reasonable estimate of the average crack-opening behavior.

III. Results

(1) Microstructure Features

Phase and grain morphology: Three quite distinct microstructures were obtained after hot pressing ABC-SiC with the different Al contents of nominally 3, 5 and 7 wt.% (Fig. 1).   In 3ABC-SiC, elongated grains corresponding to the hexagonal 4H or 6H α-SiC phases were most prevalent (Fig. 1a). Their size and shape were relatively uniform, with lengths and widths of, respectively, $l \sim 4$ to 7 μm and $w \sim 1$-2 μm, and an aspect ratio of ~5. Submicron, equiaxed SiC grains corresponding to cubic 3C β-SiC phase were also observed.

Increasing nominal Al content to 5 wt.% caused marked microstructural changes, with a bimodal structure being formed comprising a significant volume fraction of both elongated and equiaxed SiC grains (Fig. 1b). The higher Al additions in 5ABC-SiC apparently promoted anisotropic growth of the elongated grains, resulting in an aspect ratio of ~23, almost five times that of 3ABC-SiC.

This trend was continued with additional increases in Al content. In 7ABC-SiC, the aspect ratio of the elongated α-SiC grains was further increased to ~32; however, the proportion of such grains was significantly reduced with the submicron equiaxed β–SiC grains becoming predominant (Fig. 1c). Detailed microstructural characteristics for the three microstructures from Ref. [15] are summarized in Table 1.

Grain boundaries: In addition to the differing phase and grain morphology, the other major distinction in the three microstructures was in the nature of the grain boundaries. During the liquid-phase sintering, nanoscale intergranular films are typically formed between SiC grains. As reported previously [14], TEM studies revealed that the intergranular films in as-processed 3ABC-SiC were amorphous (Fig. 2) with an Al-rich composition, as determined by EDS analysis. With increasing Al content, segregation of the Al atoms to the intergranular films was found to be increased by 32% and appeared to be saturated and constant for both 5ABC and 7ABC, although considerable amounts of free Al were detected in the latter structure.

With respect to the structure of the boundaries, whereas the intergranular films were fully amorphous in 3ABC and fully crystalline in 7ABC, both amorphous and crystalline films were frequently observed in 5ABC (Fig. 2). It should be noted that epitaxial crystalline grain-boundary films were often formed on the (0001) grain-boundary surface of the matrix α-SiC grains. This epitaxial growth is attributed to the fact that one of the identified phases for the crystalline films was 2H-wurtzite, which is similar in structure to the 4H- or 6H-SiC matrix grains [14]. Because of this epitaxial growth, crystalline grain-boundary films are not always easily seen in high-resolution TEM images like the ones shown in Fig. 2; however, the consistent detection of two to three monolayers of Al segregation in the boundaries was reliably used to confirm the existence of these films.

The microstructures of the samples subjected to 72 hr exposures at 1300°C were essentially identical to those of as-hot-pressed conditions, except that the grain boundaries were all crystallized in 3, 5 and 7ABC.

(2) Fracture Toughness and Strength

Fracture Toughness: The variation in fracture toughness at 25° and 1300°C with Al wt.% is summarized in Table 2. For both as-hot-pressed and annealed 3ABC and 5ABC structures at 25°C, R-curves were determined and are shown in Fig. 3. Peak values from the R-curves indicate that in as-hot-pressed condition, 5ABC is some 17% tougher than 3ABC; both these structures are essentially twice as tough as 7ABC, which displayed a fracture toughness K_c value no greater than 4.0 MPa√m, comparable to that of commercial SiC (e.g., Hexaloy SA). Results for 3ABC and 5ABC at elevated temperatures showed a reduction in the fracture toughness at 1300°C of roughly 20 to 40%, while 7ABC had an ~20% increase. Finally, experiments using samples pre-exposed for 72 hr at 1300°C prior to room temperature testing showed that although grain-boundary crystallization occurred, there was no significant effect on the toughness (Table 2); the toughness of 3ABC and 5ABC showed a 16% increase and 26% decrease, respectively.

Strength: For comparison, ambient temperature four-point bend strength results from Ref. [15] for all three of the as-hot-pressed ABC-SiCs are given in Table 2 where each value represents the average of five measurements along with the standard deviation. All three microstructures displayed strengths near or in excess of ~500 MPa. 3ABC had a 30 to 40% higher bend strength than either the 5ABC and 7ABC structures, which showed comparable strength levels.

(3) Fatigue-Crack Growth Behavior

The variation in fatigue-crack growth rates, *da/dN*, with applied stress-intensity range, ΔK, for 3ABC- 5ABC- and 7ABC-SiC at 25° and 1300°C is shown in Fig. 4. The *da/dN* vs. ΔK data were fit to a simple Paris power-law formulation:

$$da/dN = C'\Delta K^m ,$$ (1)

where C' and m are scaling constants. Values of these constants, together with a summary of the fatigue threshold data, are listed in Table 3. All curves show very high Paris-law exponents ($m > 40$), which are typical of brittle materials, and have $K_{max,th}$ thresholds that approach 80~90% of the fracture toughness, K_c (with the exception of 7ABC). It should be noted that the Paris-law exponent for 5ABC is about twice that for 3ABC, which suggests a difference in fatigue mechanism (as discussed below).

It is apparent that fatigue-crack growth resistance scales with the fracture toughness in SiC. Considering first the ambient-temperature results, the 5ABC structure, with a $K_{max,th}$ threshold of 7.9 MPa√m, displayed the best properties followed by 3ABC, where $K_{max,th}$ ~ 5.9 MPa√m. The 7ABC structure was so brittle that it simply failed catastrophically when the ambient temperature fracture toughness was reached, i.e., when $K_{max} = K_c$ ~ 3 – 4 MPa√m; this structure showed no susceptibility to fatigue failure. With increasing temperature from 25º to 1300ºC, fatigue thresholds were reduced for 3ABC and 5ABC, reflecting the lower toughnesses at high temperature; however, the Paris-law exponents were very similar to their room temperature values, which is indicative of similar damage mechanisms being active at low and high temperatures.

(4) Fractography and Crack Paths

Overload fracture surfaces from the fracture toughness samples show a transition of increasing transgranular fracture with increasing Al content from 3 to 7 wt.% (Fig. 5); however, even for 7ABC there is still some intergranular fracture between the fine grains. SEM micrographs of the crack-path trajectories in Fig. 6a confirms the intergranular fracture mode in 3ABC, and provides evidence that crack-tip shielding by individual grain bridging (frictional bridging) in the crack wake is the primary toughening mechanism in this structure, as reported in refs. [7-11]. This mechanism of grain bridging pertains to behavior in 3ABC at both the low and high temperatures (Fig. 6b). Crack bridging is also apparent in the 5ABC structure at both 25° and 1300°C; however, the primary mechanism is quite different (Fig. 6c-f). Here, the majority of bridges are composed of uncracked ligaments of SiC which span the crack wake. Uncracked-ligament bridging is a toughening mechanism observed in many materials, including metal-matrix composites [22], γ-based TiAl intermetallics [23], and even human bone

11

[24]. Such ligaments were typically composed of one or more elongated grains; indeed, the crack path in both the 3ABC and 5ABC microstructures appeared to preferentially seek out these α-SiC grains. In contrast, the crack path in the as-processed 7ABC microstructure is predominantly transgranular through both the equiaxed and elongated grains, with no evidence of any form of bridging.

Corresponding fatigue fracture surfaces for the 3ABC and 5ABC structures were essentially identical to the overload fracture surfaces, except for the presence of debris. Such observations are consistent with the generally accepted mechanisms for the fatigue of grain-bridging ceramics, involving (i) damage (crack-advance) mechanisms ahead of the crack tip essentially identical to those under monotonic (non-cyclic) loading, and (ii) the progressive degradation of grain bridging with cyclic loading behind the crack tip, associated with such processes as frictional wear in the sliding grain boundaries and the cracking/crushing of crack-surface asperities [7,25,26].

As noted above, fracture surfaces and crack paths at 1300˚C are of similar nature to that at room temperatures, with clear evidence of grain bridging and no evidence of creep damage in the form of softening of the intergranular films and resulting grain-boundary cavitation. This is apparent from high magnification TEM images of the crack-tip regions in 3ABC and 5ABC after fatigue-crack growth at high temperatures (Fig. 7). Indeed, based on the fractographic characterization and the results presented in Figs. 6 and 7, we can conclude that the mechanisms of fracture and fatigue-crack propagation in both these microstructures are essentially unchanged between 25° and 1300°C.

(5) Crack-Opening Profile Results

Clearly, both toughening and fatigue-crack growth in the 3ABC and 5ABC structures are markedly influenced by the presence of crack bridging. In order to verify the existence of such crack-tip shielding, crack-opening profiles were measured for two cracks in samples used for R-curve testing, which were then loaded *in situ* in the field-emission SEM to a stress intensity of 6.2 MPa√m; results are shown in Fig. 8 and are compared with the computed crack-opening profile for an elastic traction-free crack at the same applied *K*. In this figure, it can be seen that measured crack openings are significantly smaller than that expected for a traction-free crack, clearly implying the

presence of crack bridging in both samples. Furthermore, the crack in the 5ABC-SiC sample has a smaller opening than that for the 3ABC-SiC sample, indicative of more potent bridging in the 5ABC microstructure.

These differences in the degree of crack bridging can be quantified by fitting the near-tip crack-opening profile to the Irwin crack-opening displacement solution for a linear elastic crack in order to obtain the near-tip stress intensity, K_{tip}:

$$u_{tot}(x) = \frac{K_{tip}}{E'} \sqrt{\frac{8(a-x)}{\pi}} \quad, \tag{2}$$

where E' is Young's modulus (E in plane stress, $E/(1-v^2)$ in plane strain, where v is Poisson's ratio), and x is the position of interest with origin at the load line. Regressions of the crack-tip opening profile data for the first 70 μm after the crack tip yield a value of 2.5 MPa√m for 3ABC and 1.6 MPa√m for 5ABC. Accordingly, considering that K_{tip} may be expressed as:

$$K_{tip} = K_{app} - K_{br} \quad, \tag{3}$$

where K_{app} is the applied stress intensity (6.2 MPa√m) and K_{br} is the contribution due to bridging, K_{br} is determined to be 3.7 MPa√m for 3ABC and 4.6 MPa√m for 5ABC. It should be noted that, at the same applied stress intensity, the 5ABC microstructure develops the higher contribution from bridging, and the lower driving force experienced at the crack tip.

IV. Discussion

(1) Toughening Mechanisms

Characterization of the observed crack paths (Fig. 6) along with the crack opening profile measurements (Fig. 8) affirm that crack bridging is the primary toughening mechanism in 3ABC and 5ABC-SiC; in contrast, no bridging was observed in the as-processed 7ABC microstructure which had the lowest fracture toughness, comparable to that of commercial silicon carbides. For 3ABC-SiC, frictional bridging appears to be dominant whereby bridging stresses are developed by the frictional resistance to pullout and mechanical interlocking of grains which interact across the crack wake,

13

schematically shown in Fig. 9a. Such frictional grain bridging is a common toughening mechanism for a variety of ceramic materials which fracture intergranularly [7,27-30].

Conversely, observations of cracking in the 5ABC microstructure indicate a change in toughening mechanism to uncracked-ligament, or elastic, bridging; with this change in mechanism there is an associated increase in toughness. As seen in Fig. 6c,d,e, uncracked ligaments, often several grains in size, were observed to bridge the crack wake in the 5ABC microstructure; frictional bridges, such as those seen in 3ABC (Fig 6a,b), were far less common. Such ligaments apparently form as a result of local crack arrest at microstructural inhomogeneities, which leaves unfractured ligaments in the crack wake, due to either non-uniform advance of the crack front or crack nucleation ahead of the main crack tip; this phenomenon is illustrated in Fig 9b. However, it is currently unclear what causes the transition from predominantly frictional to uncracked-ligament bridging, although this change must be related to the notable differences in microstructure and to the grain-boundary film properties. Specifically, the dominant local arresting points responsible for the formation of such uncracked ligaments may be attributed to large elongated grains oriented favorable for local crack deflection, as illustrated in Fig. 9b, and/or to spatial variations in grain boundary strengths due to structure[2] or chemistry differences. Since the crack path follows the elongated grains almost exclusively, the higher aspect ratio and smaller fraction of elongated grains in the 5ABC, as compared to the 3ABC, structure undoubtedly promotes larger off-angle deflections as the crack propagates along the boundary of the α–SiC grains; thus, with the next α grain further away than in the 3ABC SiC, uncracked ligaments are more probable, as shown schematically in Fig. 9b. Uncracked-ligament bridges are expected to be more potent than frictional bridges in that they should be able to sustain higher loads before failing. This is consistent with the higher toughness and the higher deduced bridging stress intensity, K_{br}, of the 5ABC structure (described above), both of which confirm the enhanced degree of bridging where uncracked ligaments predominate.

Finally, the behavior of 7ABC is illustrated in Fig. 9c. Here, unlike the 3ABC and 5ABC microstructures, the crack path is predominantly transgranular, and proceeds

---

[2] While amorphous and the 2H-wurtzite crystalline phase has been positively identified for some boundaries, other boundary structures may also exist.

through both the equiaxed β and elongated α–SiC grains, with very few cases of intergranular fracture. With such a cracking morphology, there was no evidence of any form of bridging.

The fracture toughness values for both 3ABC- and 5ABC-SiC are slightly lower at 1300°C than their corresponding room temperature values, which is in agreement with previous results on 3ABC-SiC [9]. Such a drop in toughness may be related to changes in the residual stress state, either by the relaxation of thermal mismatch stresses which, along with mechanical interlocking, may contribute to the tractions acting on the frictional bridges [28,31,32], or by altering the mismatch stresses in triple point junctions, which has been shown to affect the toughness of silicon nitride [33]. It should be noted that 3ABC-SiC, which has a larger proportion of frictional bridges, experiences a larger drop in toughness compared to 5ABC-SiC. Such a result is consistent with a reduction in thermal stresses affecting the frictional bridging tractions, suggesting that the former mechanism indeed plays a role here.

While exposure to 1300°C is known to affect the microstructure of ABC-SiCs, by the crystallization of amorphous grain boundaries, along with associated chemistry changes, and the formation of nano-precipitates within the SiC grains [14,34], only minor effects on the subsequent low-temperature toughness were evident. Thus, it may be concluded that although the crystalline boundaries have a very positive impact on the high-temperature creep resistance of 3ABC and 5ABC silicon carbides [13], either amorphous or crystalline boundaries are sufficiently brittle to give intergranular fracture and hence high toughness in these materials at lower temperatures (see also ref. [10]).

Finally, it should be noted that although the 5ABC microstructure has the highest toughness, it also has the lowest strength (Table 2). This inverse dependence of strength and toughness may be attributed to the fact that 5ABC-SiC has a larger (elongated) grain size, and correspondingly is expected to have larger initial flaw sizes. Although 7ABC-SiC has the lowest toughness, its strength is comparable to that of 5ABC-SiC, again from smaller initial flaw sizes due to the smaller grains. The 3ABC microstructure achieves its relatively high fracture toughness with the smallest grain size, and accordingly, has the highest strength of the three microstructures.

(2) Cyclic Fatigue Mechanisms

Since the fatigue of brittle materials such as SiC is invariably controlled by the progressive degradation under cyclic loading of the prevalent extrinsic toughening (crack-tip shielding) mechanisms, a sound strategy for improving resistance to fatigue-crack growth is by making the shielding mechanisms more resilient in the presence of such cyclic loads. In this regard, in addition to providing increased toughening, uncracked-ligament bridges are significantly less susceptible to fatigue damage during cyclic loading since the cycle-dependent interfacial wear mechanisms that occur to degrade frictional bridges [26] are not relevant. Instead of wear of the sliding boundaries, the degradation of the uncracked-ligament bridges must occur by a fracture process, presumably when a critical failure stress is reached, a mechanism that is likely to be cycle-independent. Indeed, a reduced susceptibility to cyclic fatigue was observed in 5ABC-SiC, which is toughened primarily by such ligament bridging, as reflected by the much higher Paris-law exponents (i.e., steeper da/dN-ΔK curves) (Table 3). This was especial apparent at 1300°C where fatigue data was unattainable for the 5ABC microstructure over much of the range of crack-growth rates due to unstable fracture of the specimens.

Thus, by increasing the Al content in ABC-SiC to ~5 wt.%, which leads to a microstructure of high aspect-ratio α-SiC grains with both amorphous and crystalline grain-boundary films, which in turn causes a change in the predominant crack-tip shielding mechanism from frictional to uncracked-ligament bridging, optimal crack-growth resistance at 25° and 1300°C can be obtained under both monotonic and cyclic loading. Not only is the ligament bridging mechanism a more potent mode of toughening in ABC silicon carbides, but it also is more resistant to degradation under cyclic loading and thus leads to a reduced susceptibility to fatigue failure.

V. Conclusions

An experimental study has been made of the microstructural and mechanistic origins of the fracture toughness and fatigue-crack growth resistance of a series of Al-containing ABC-silicon carbides at 25° and 1300°C, the following conclusions can be made:

(1) Of the three silicon carbides examined here (3, 5, and 7ABC SiC), 5ABC-SiC demonstrated the highest peak toughness of 8.9 MPa√m at 25°C and 7.1 MPa√m at 1300°C. These high toughness values were attributed to crack-tip shielding, primarily from *uncracked-ligament* bridging in the crack wake. Corresponding toughening in 3ABC-SiC was primarily associated with *frictional* grain bridging; this structure displayed roughly 15% lower toughness. No bridging was detected in 7ABC microstructure, which accordingly exhibited the lowest toughness, comparable to that of commercial SiC.

(2) Whereas the 7ABC structure was too brittle to be susceptible to fatigue, 3ABC and 5ABC exhibited cyclic fatigue-crack growth at stress intensities above a $K_{max,th}$ threshold which was roughly 80 – 90% of the peak toughness.

(3) Fatigue-crack growth in 3ABC and 5ABC was associated the suppression of crack bridging in the crack wake. In general, the 5ABC microstructure was less susceptible to fatigue, as evidenced by its steeper *da/dN-ΔK* curve. This was attributed to the higher resilience of uncracked-ligament bridging to degradation under cyclic loading, as compared to frictional grain bridging in 3ABC.

(4) While both the fracture toughness values and fatigue thresholds for 3 and 5ABC-SiC were found to be lower at 1300°C, the mechanisms of toughening and fatigue-crack propagation were found to be the same as at 25°C. No evidence of creep cavitation damage was detected during the fatigue testing at 1300°C.

References

[1] Kim DH, Kim CH. J. Am. Ceram. Soc. 1990;73:1431.
[2] Mitchell Jr TD, De Jonghe LC, MoberlyChan WJ, Ritchie RO. J. Am. Ceram. Soc. 1995;78:97.
[3] Cao JJ, MoberlyChan WJ, De Jonghe LC, Gilbert CJ, Ritchie RO. J. Am. Ceram. Soc. 1996;79:461.
[4] Padture NP. J. Am. Ceram. Soc. 1994;77:519.
[5] Padture NP, Lawn BR. J. Am. Ceram. Soc. 1994;77:2518.
[6] Lee SK, Kim CH. J. Am. Ceram. Soc. 1994;77:1655.
[7] Gilbert CJ, Cao JJ, MoberlyChan WJ, De Jonghe LC, Ritchie RO. Acta Metall. Mater. 1996;44:3199.
[8] Gilbert CJ, Ritchie RO. Acta Mater. 1998;46:609.
[9] Chen D, Gilbert CJ, Zhang XF, Ritchie RO. Acta Mater. 2000;48:659.
[10] Chen D, Zhang XF, Ritchie RO. J. Am. Ceram. Soc. 2000;83:2079.
[11] Chen D, Sixta ME, Zhang XF, De Jonghe LC, Ritchie RO. 2000, 4599.
[12] Ritchie RO. Int. J. Fract. 1999;100:55.
[13] Sixta M, Zhang XF, De Jonghe LC. J. Am. Ceram. Soc. 2001;84:2022.
[14] Zhang XF, Sixta M, De Jonghe LC. J. Am. Ceram. Soc. 2000;83:2813.
[15] Zhang XF, Yang Q, De Jonghe LC. Acta Mater. 2003;51:3849.
[16] Ruska J, Gauckler LJ, Lorenz JL, Rexer HU. J. Mater. Sci. 1979;14:2013.
[17] Dauskardt RH, Ritchie RO. Closed Loop 1991;17:7.
[18] Murakami Y. Stress Intensity Factors Handbook. Pergamon Press, 1987. p. 640.
[19] Ritchie RO, Yu W. Small Fatigue Cracks. Ritchie RO, Lankford J, Ritchie RO, Lankford JRitchie RO, Lankford Js. TMS-AIME, Warrendale, PA,1986, 167.
[20] Gilbert CJ, McNaney JM, Dauskardt RH, Ritchie RO. J. Test. Eval. 1994;22:117.
[21] Chen D, Gilbert CJ, Ritchie RO. J. Test. Eval. 2000;28:236.
[22] Shang JK, Ritchie RO. Metall. Trans. 1989;20A:897.
[23] Chan KS. Metall. Trans. 1993;24A:569.
[24] Nalla RK, Kinney JH, Ritchie RO. Nature Materials 2003;2:164.
[25] Gilbert CJ, Dauskardt RH, Ritchie RO. J. Am. Ceram. Soc. 1995;78:2291.
[26] Lathabai S, Rödel J, Lawn B. J. Am. Ceram. Soc. 1991;74:1348.
[27] Swanson PL, Fairbanks CJ, Lawn BR, Mai Y-W, Hockey BJ. J. Am. Ceram. Soc. 1987;70:279.
[28] Bennison SJ, Lawn BR. Acta Metall. 1989;37:2659.
[29] Mai Y-W, Lawn BR. J. Am. Ceram. Soc. 1987;70:289.
[30] Li C-W, Lee D-J, Lui S-C. J. Am. Ceram. Soc. 1992;75:1777.
[31] Swain MV. J. Mater. Sci. Lett. 1986;5:1313.
[32] Kokaly MT, Tran DK, Kobayashi AS, Dai X, Patel K, White KW. Mater. Sci. Eng. 2000;A285:151.
[33] Pezzotti G, Kleebe H-J. Journal of the European Ceramic Society 1999;19:451.
[34] Zhang XF, Sixta ME, Chen D, De Jonghe LC. J. Mater. Sci. 2001;36:5447.

Table 1. Comparison of Microstructures of ABC-SiC (after Ref. [15])

		3ABC-SiC	5ABC-SiC	7ABC-SiC
Grain Structures		Uniform long	Bimodal	Equiaxed*
Grain Size (μm) & Aspect Ratio	Elongated Grains	$l = 4.4 \pm 1.4$ $w = 1.0 \pm 0.3$ $l/w = 4.7 \pm 0.6$	$l = 20 \pm 6.4$ $w = 0.8 \pm 0.3$ $l/w = 23.2 \pm 6.8$	$l = 11.5 \pm 5.8$ $w = 0.4 \pm 0.2$ $l/w = 31.6 \pm 15.4$
	Equiaxed		0.6 ± 0.2	0.6 ± 0.3
Area Density of Elongated Grains (mm^{-2})		85,000	45,000	23,000
Phase & Volume Fraction		70% 4H 30% 3C	12% 4H, 21% 6H 67% 3C	20% 6H 80% 3C
Grain Boundaries		Amorphous	Partially crystallized	Fully crystallized

*With only a few elongated (needle-like) grains

Table 2. Comparison of Mechanical Properties of ABC-SiC

	3ABC-SiC	5ABC-SiC	7ABC-SiC
Strength at 25˚C, (Ref. [15]) 4-pt bending (MPa)	691 ± 12	480 ± 30	533 ± 58
Toughness K_c at 25˚C (MPa√m)	7.6	8.9	4.0* (upper bound)
Toughness K_c at 1300˚C (MPa√m)	4.5	7.4	4.9* (upper bound)
Toughness K_c of pre-exposed samples at 25˚C (MPa√m)	8.8	6.6	—

*Toughness evaluated from a razor micro-notch.

Table 3. Cyclic fatigue-crack growth properties for ABC-SiC tested at R=0.1, ν=25Hz

	Testing Temperature (˚C)	Fatigue Thresholds ΔK_{th} (MPa√m)	$K_{max,th}$ (MPa√m)	Critical Toughness, K_c (MPa√m)	$K_{max,th}/K_c$	Paris Law $da/dN = C'\Delta K^m$ m	C'
3ABC	25°	5.3	5.9	7.6	0.78	45	4.4×10^{-41}
	1300°	3.5	3.9	4.5	0.87	44	4.3×10^{-34}
5ABC	25°	7.1	7.9	8.9	0.88	133	9.5×10^{-124}
	1300°	6.1	6.8	7.4	0.92	107	3.7×10^{-95}

List of Figure Captions

Fig. 1.   SEM micrographs of etched surfaces of ABC-silicon carbides, showing the characteristic grain structures: (a) uniformly elongated grains in 3ABC, (b) bimodal structure of elongated (α-SiC) and equiaxed (β-SiC) in 5ABC, and (c) equiaxed grains with sparsely distributed needle-like grains in 7ABC. (Courtesy of Q. Yang)

Fig. 2. High-resolution TEM micrographs showing the nature of the grain-boundary films in hot-pressed SiC with different Al content, showing (a) amorphous films in 3ABC, (b) fully crystallized films in 7ABC, and (c) amorphous, (d) partially crystallized and (e) fully crystallized films in 5ABC.   Fig. 3.   Crack-growth resistance, K_R, curves, plotted as a function of crack extension, Δa, for as-hot-pressed xABC-SiC at room temperature.

Fig. 4.   Cyclic fatigue-crack growth rates, da/dN, at $R = 0.1$ in ABC-SiC, as a function of the applied stress-intensity range, ΔK, at temperatures of 25˚ and 1300˚C.   Note that 7ABC is sufficiently brittle that it exhibits no subcritical crack growth, i.e., it fails catastrophically once $K_{max} > K_c$; the dashed curve for this structure is drawn where $K_{th,max} = K_c$.

Fig. 5.   SEM micrographs of the overload fracture surfaces of (a) 3ABC-, (b) 5ABC- and (c) 7ABC-SiC.   Fracture in 3ABC and 5ABC is intergranular, whereas it is predominantly transgranular in 7ABC.

Fig. 6.   SEM micrographs of metallographic sections taken perpendicular to the fracture surface showing the crack paths during fatigue-crack growth at 25˚C and 1300˚C for 3ABC (a,b) and 5ABC-SiC (c-f). Frictional bridging (a,b,f) was most common in 3ABC while uncracked-ligament bridges (c,d,e) were predominant in 5ABC. The horizontal arrows indicate the general direction of crack growth.

Fig. 7.   Transmission electron micrographs near the crack tip in (a) 3ABC, and (b, c) 5ABC grown under cyclic loading at 1300˚C ($R = 0.1$, $\nu = 25$ Hz). Note in (b) the equiaxed grains also fracture intergranularly and in (c) a failure of uncracked ligament. Large arrows indicate the general direction of crack propagation, and small arrows point to the primary cracks near the crack tip.

Fig. 8.   Comparison of the crack-opening profiles for a monotonically-loaded crack in the 3ABC and 5ABC microstructure after R-curve testing. Samples were loaded *in situ* in a field-emission FESEM to an applied driving force of 6.2 MPa√m. The inset shows the curve fit for the first 70 μm behind the crack tip, where the solid line is for 5ABC (K_{tip}=1.6 MPa√m), and the broken line for 3ABC (K_{tip}=2.5 MPa√m).

Fig. 9. Schematic illustrations of how the crack paths lead to the development (or not) of crack bridging in (a) 3ABC, (b) 5ABC, and (c) 7ABC-SiC. Note how the predominant mode of bridging in 3ABC is from frictional grain bridging, whereas it results more from uncracked ligaments in 5ABC; in contrast, no bridging is developed in the 7ABC.
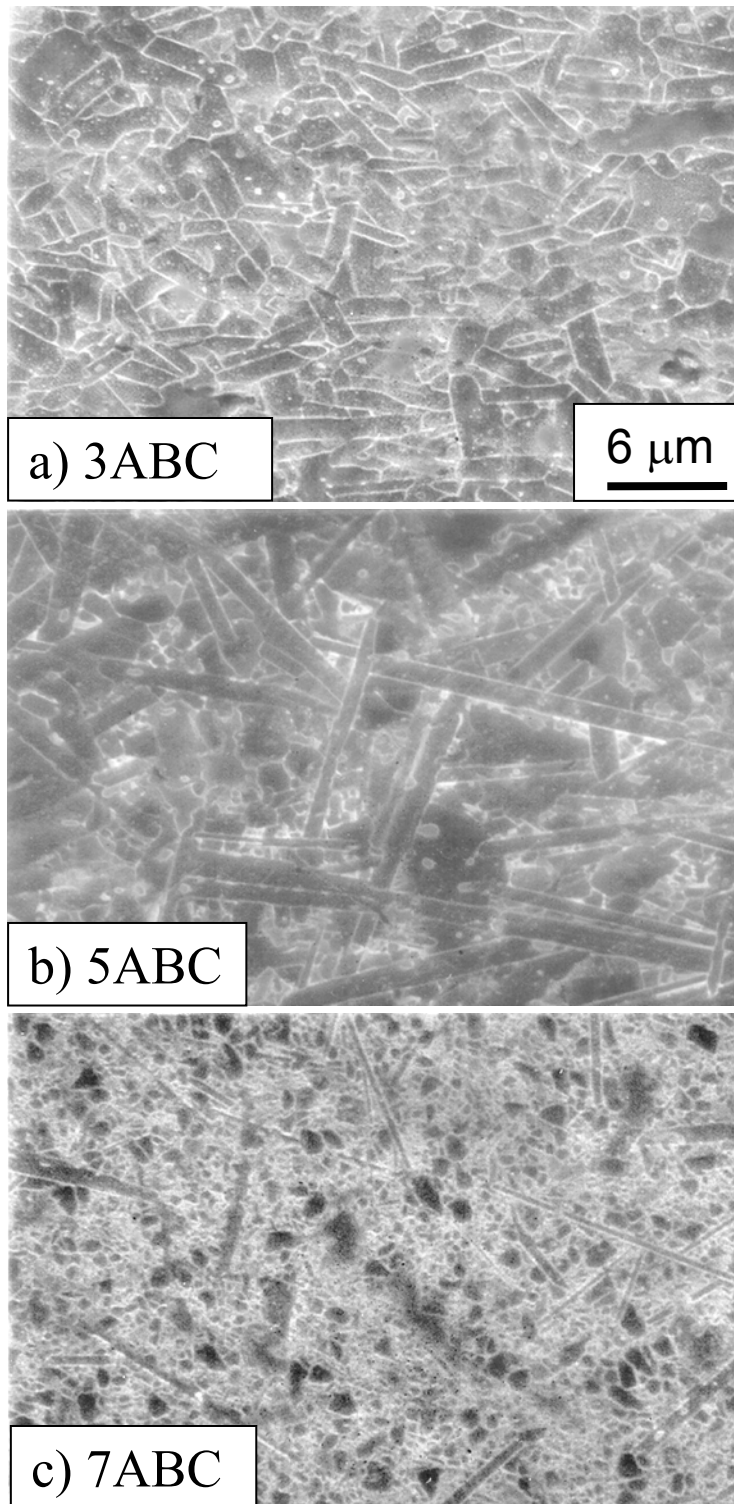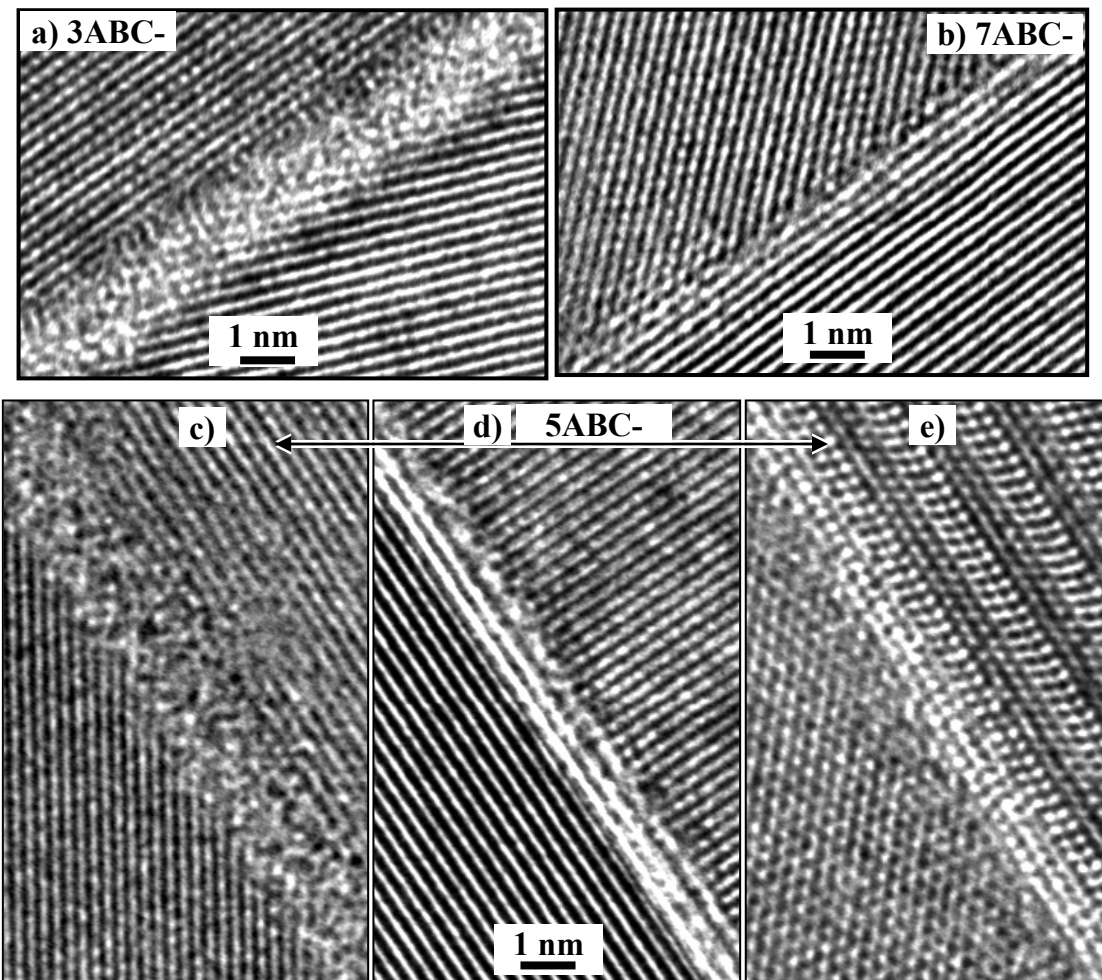
Fig. 1. SEM micrographs of etched surfaces of ABC-silicon carbides, showing the characteristic grain structures: (a) uniformly elongated grains in 3ABC, (b) bimodal structure of elongated (α-SiC) and equiaxed (β-SiC) in 5ABC, and (c) equiaxed grains with sparsely distributed needle-like grains in 7ABC. (Courtesy of Q. Yang)

Fig. 2. High-resolution TEM micrographs showing the nature of the grain-boundary films in hot-pressed SiC with different Al content, showing (a) amorphous films in 3ABC, (b) fully crystallized films in 7ABC, and (c) amorphous, (d) partially crystallized and (e) fully crystallized films in 5ABC.
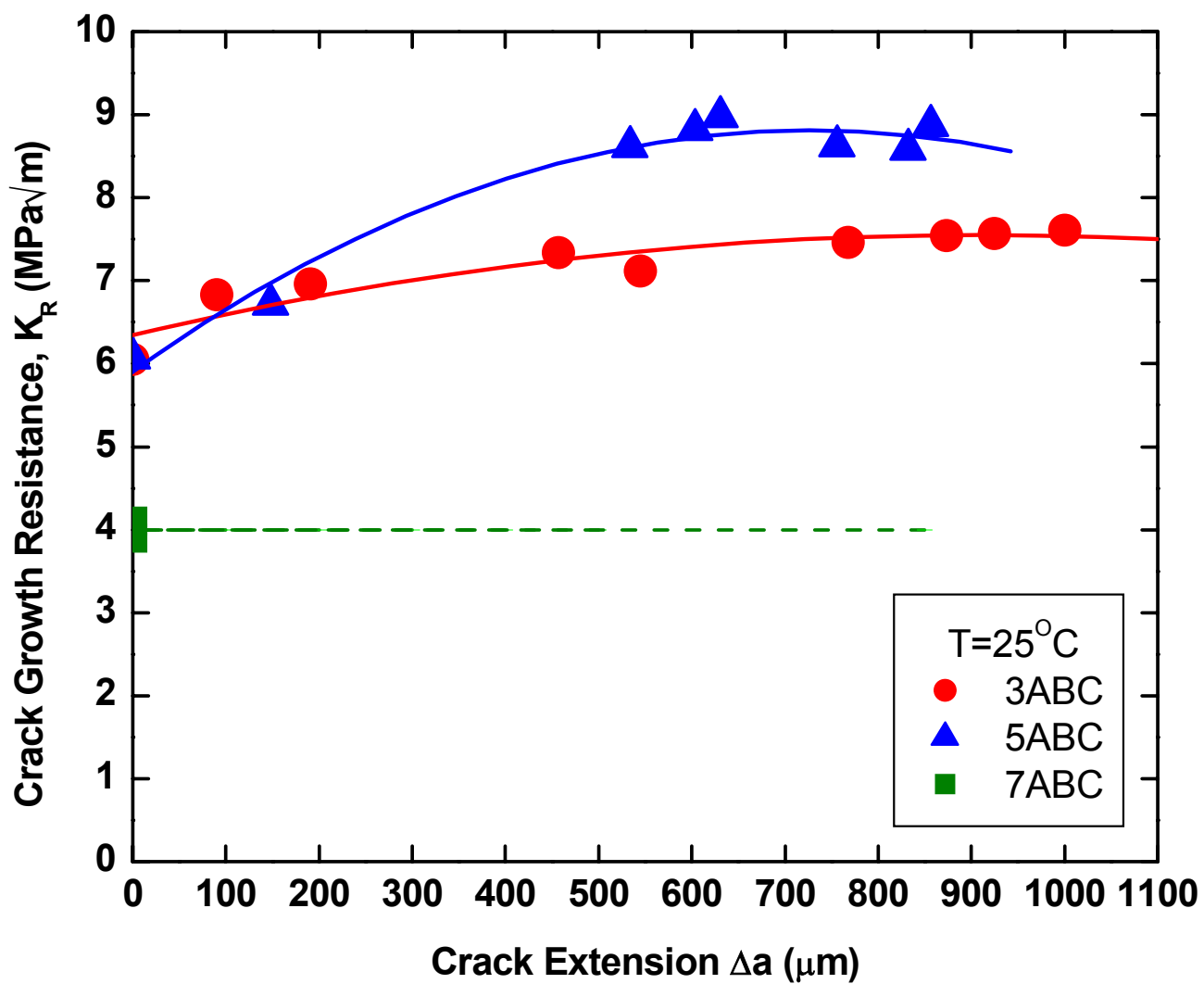
Fig. 3.   Crack growth resistance, K_R, plotted as a function of crack extension, Δa, for as-hot-pressed xABC-SiC at room temperature.
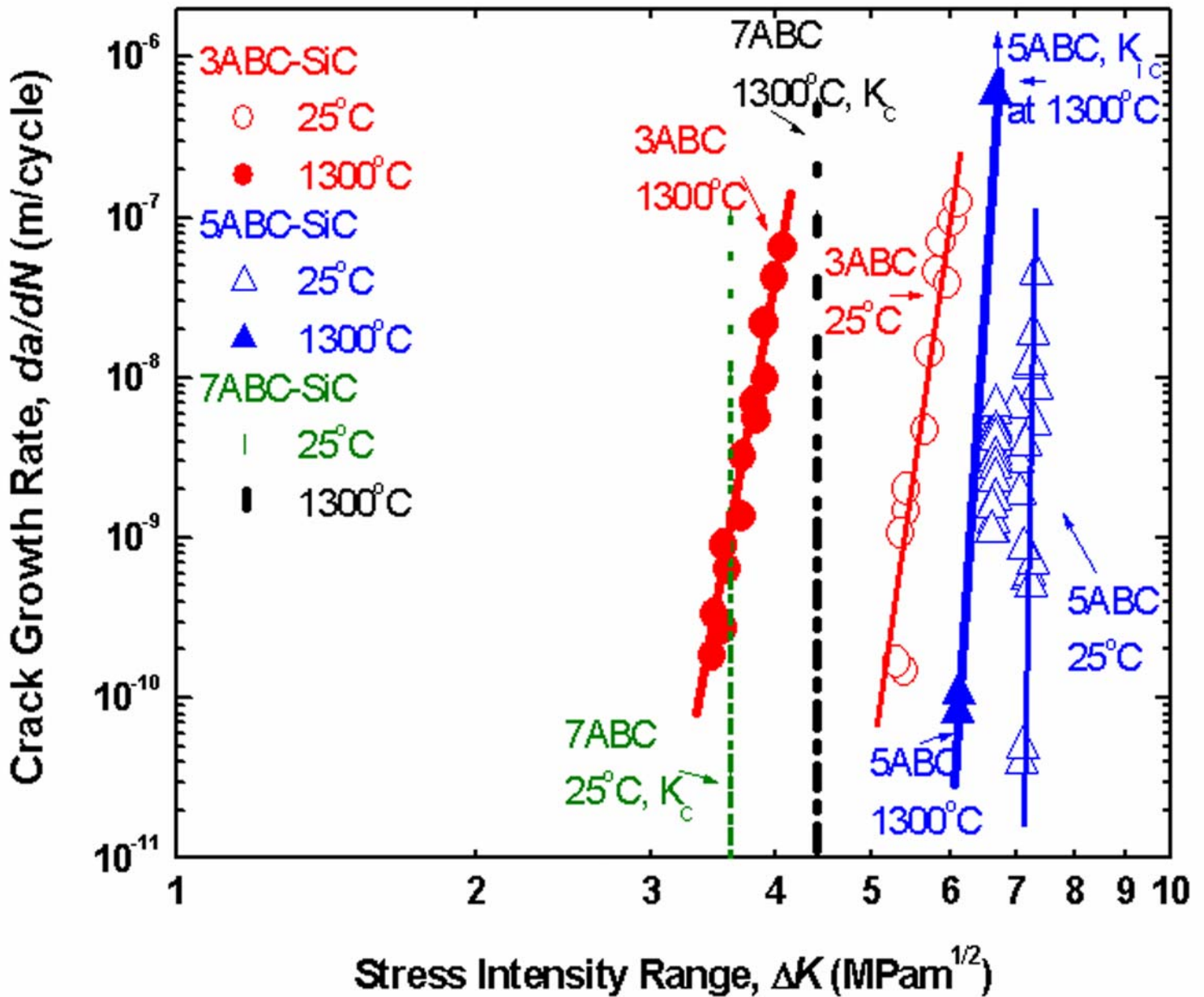
Fig. 4. Cyclic fatigue-crack growth rates, *da/dN*, at *R* = 0.1 in ABC-SiC, as a function of the applied stress-intensity range, ΔK, at temperatures of 25˚ and 1300˚C. Note that 7ABC is sufficiently brittle that it exhibits no subcritical crack growth, i.e., it fails catastrophically once $K_{max} > K_c$; the dashed curve for this structure is drawn where $K_{th,max} = K_c$.
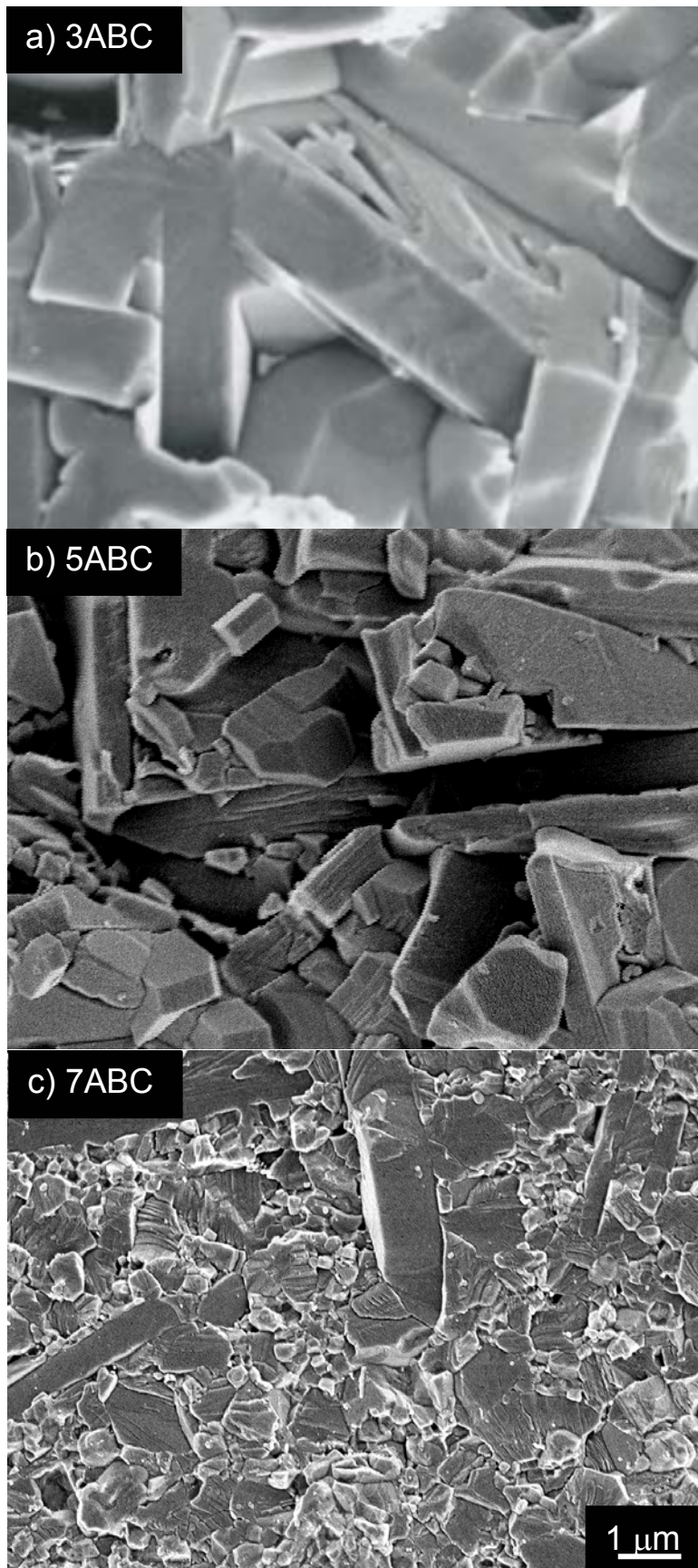
Fig. 5. SEM micrographs of the overload fracture surfaces of (a) 3ABC-, (b) 5ABC- and (c) 7ABC-SiC. Fracture in 3ABC and 5ABC is intergranular, whereas it is predominantly transgranular in 7ABC.
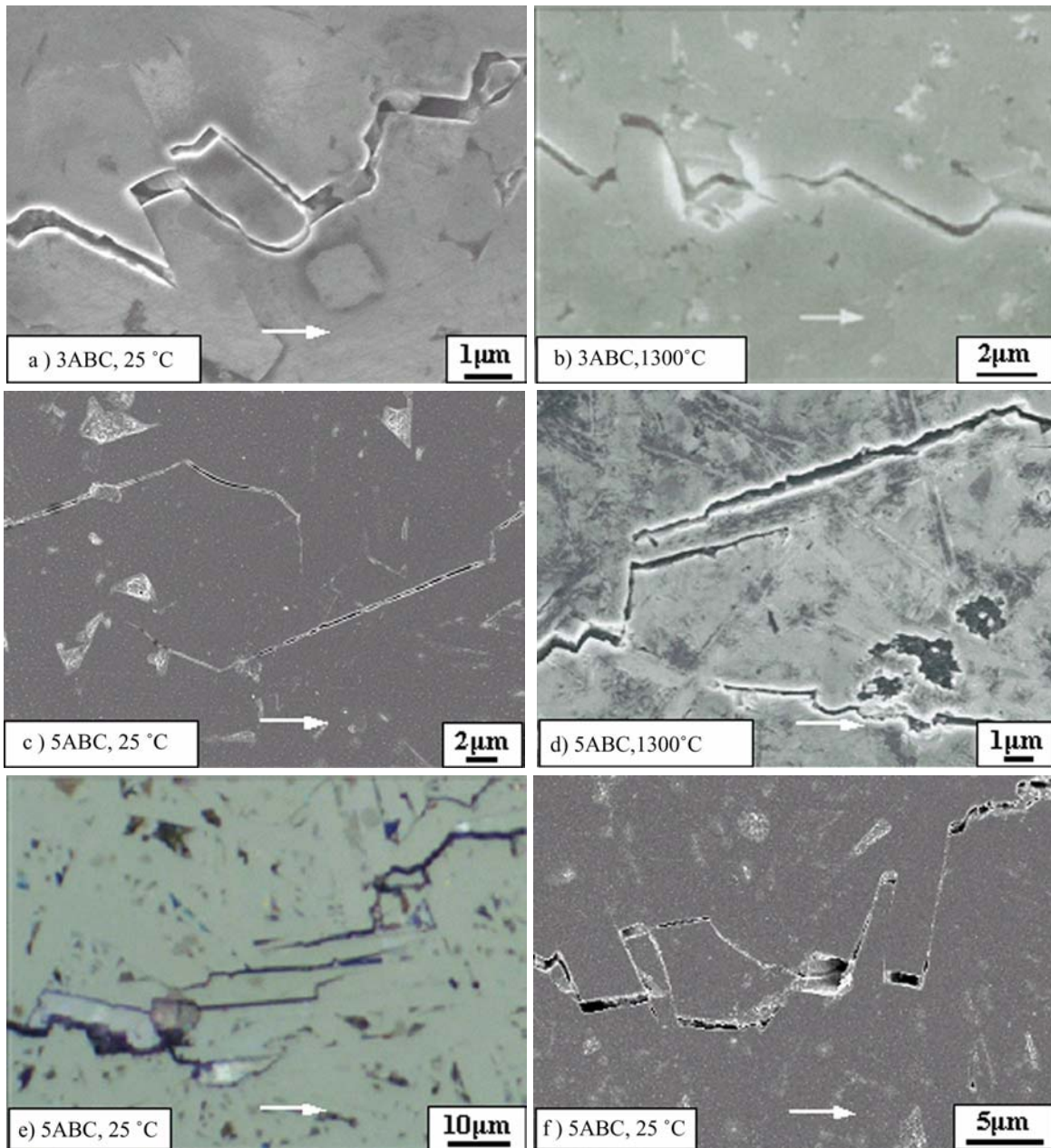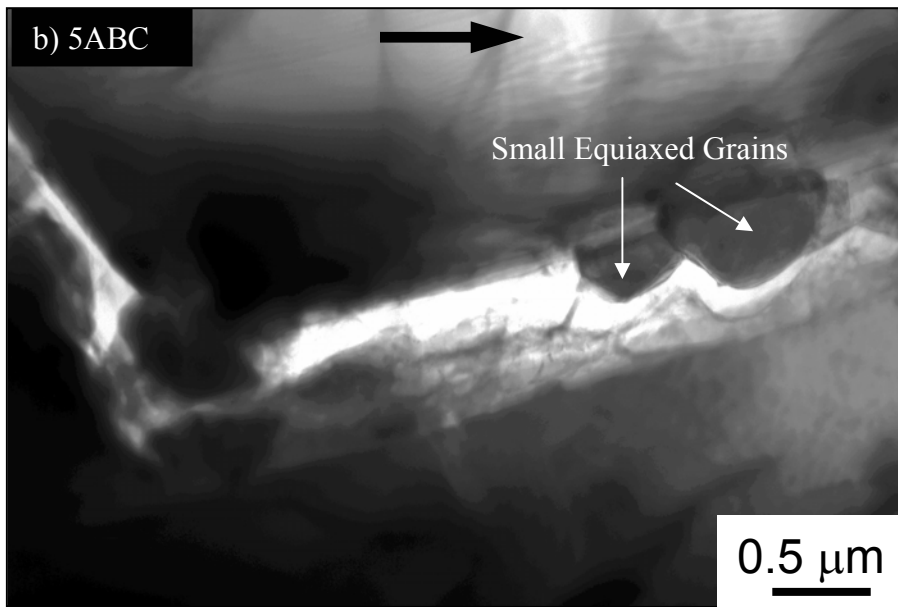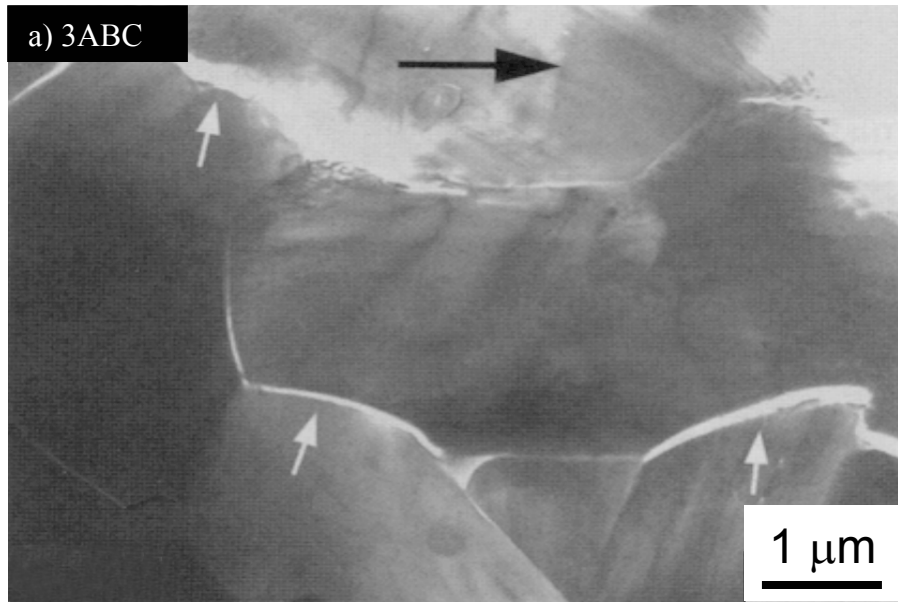
Fig. 6. SEM micrographs of metallographic sections taken perpendicular to the fracture surface showing the crack paths during fatigue-crack growth at 25˚C and 1300˚C for 3ABC (a,b) and 5ABC-SiC (c-f). Frictional bridging (a,b,f) was most common in 3ABC while uncracked ligament bridges (c,d,e) were predominant in 5ABC. The horizontal arrows indicate the general direction of crack growth.
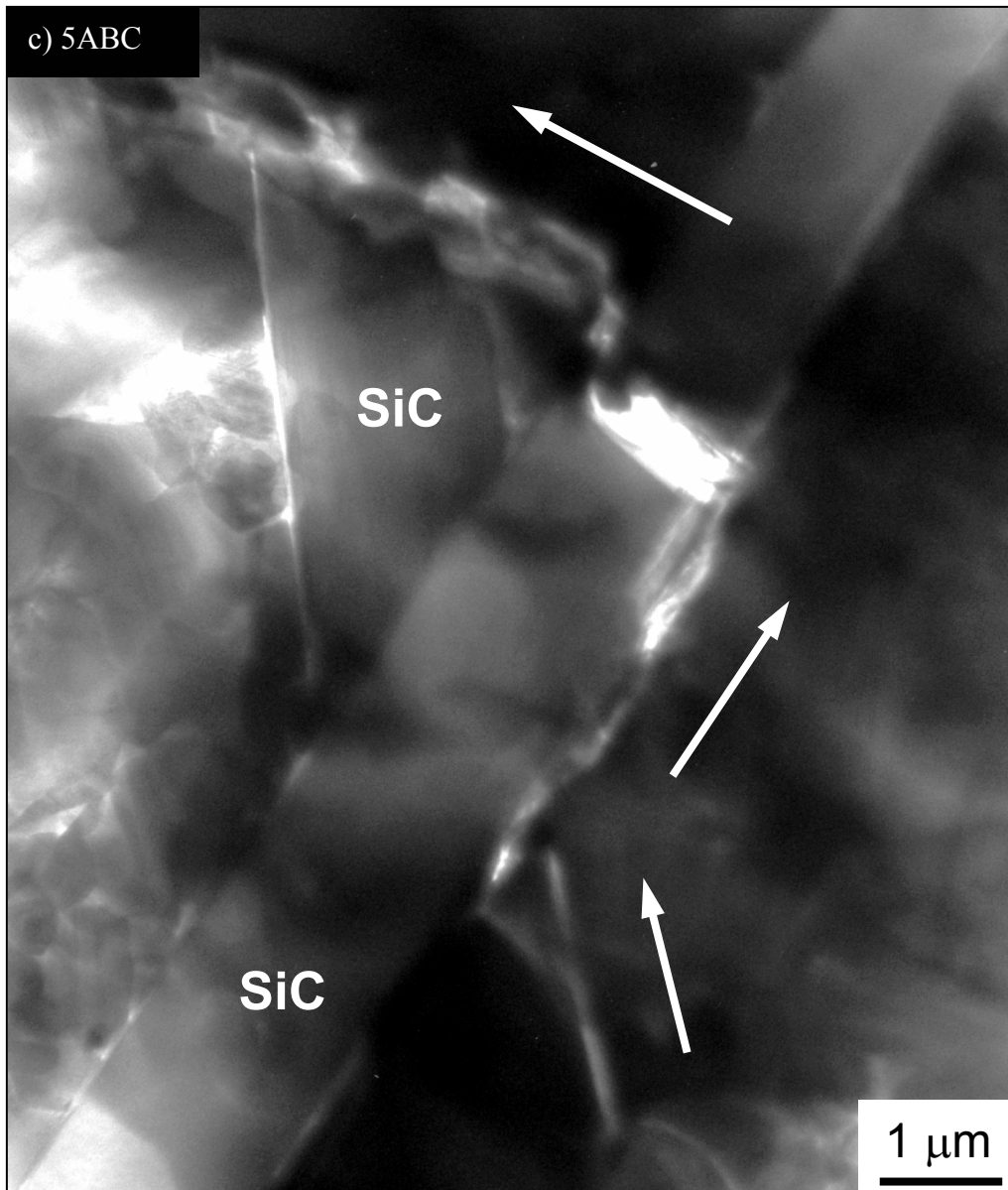
a) 3ABC

1 μm

b) 5ABC

Small Equiaxed Grains

0.5 μm

Fig. 7. Transmission electron micrographs near the crack tip in (a) 3ABC, and (b, c) 5ABC grown under cyclic loading at 1300°C ($R = 0.1$, $v = 25$ Hz). Note in (b) the equiaxed grains also fracture intergranularly and in (c) a failure of uncracked ligament. Large arrows indicate the general direction of crack propagation, and small arrows point to the primary cracks near the crack tip.
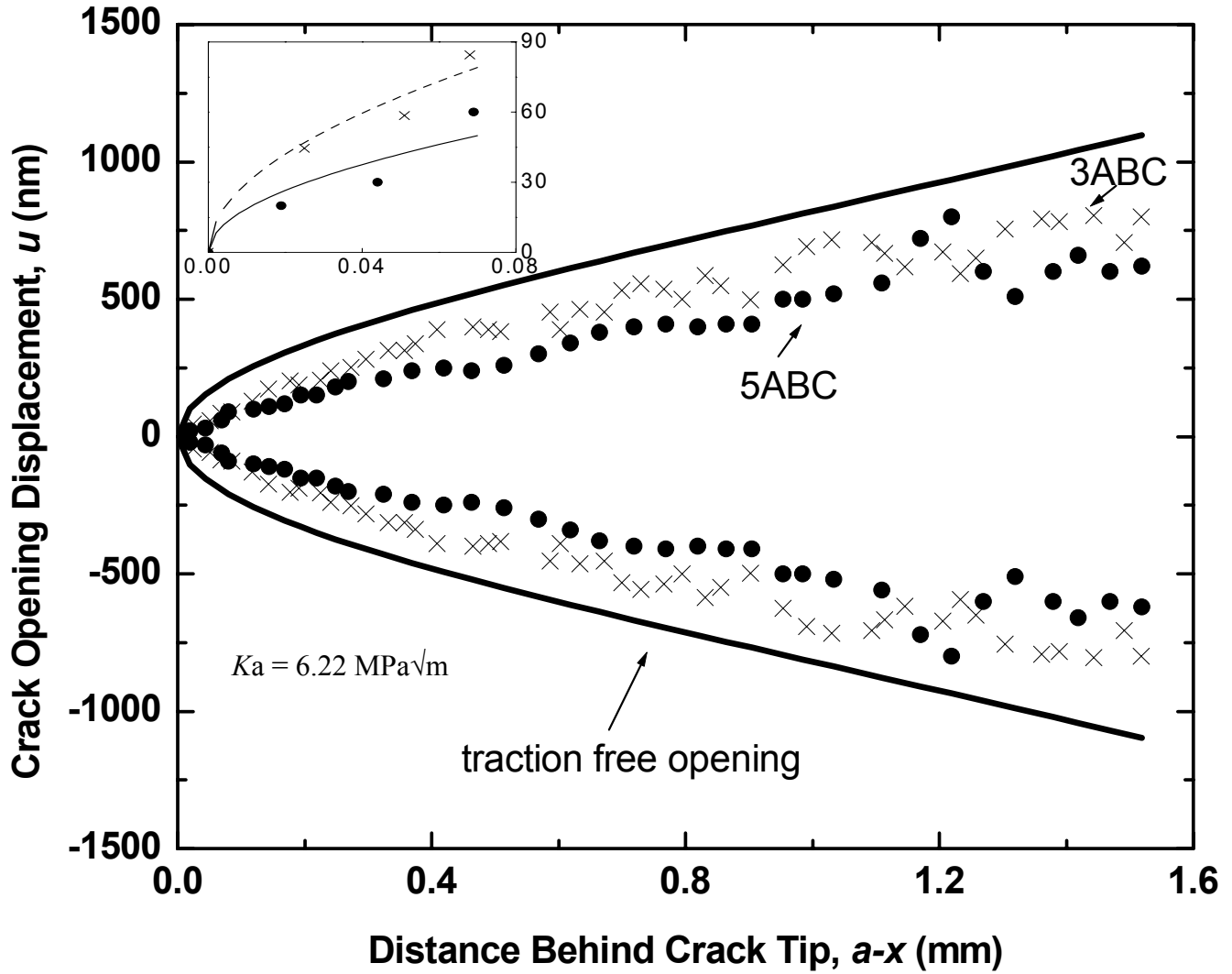
Fig. 8. Comparison of the crack-opening profiles for a monotonically-loaded crack in the 3ABC and 5ABC microstructure after R-curve testing. Samples were loaded *in situ* in a field-emission FESEM to an applied driving force of 6.2 MPa√m. The inset shows the curve fit for the first 70 μm behind the crack tip, where the solid line is for 5ABC (K_{tip}=1.6 MPa√m), and the broken line for 3ABC (K_{tip}=2.5 MPa√m).

3 ABC: moderate aspect ratio grains at high volume fraction
frictional pull-out dominates
high toughness

Full frictional pull-out

Fracture-friction mode

friction facet

friction facets

1μm

a

5 ABC: elongated grain size moderate volume fraction:
formation of elastic bridging ligaments
highest toughness

local crack path

uncracked ligament

local crack path

σ

elastic bridge

mean crack path

1μm

b

7 ABC: Highly elongated grain size at low volume fraction:
transgranular fracture
no bridging
low toughness

local crack path

α-SiC

σ

β-SiC

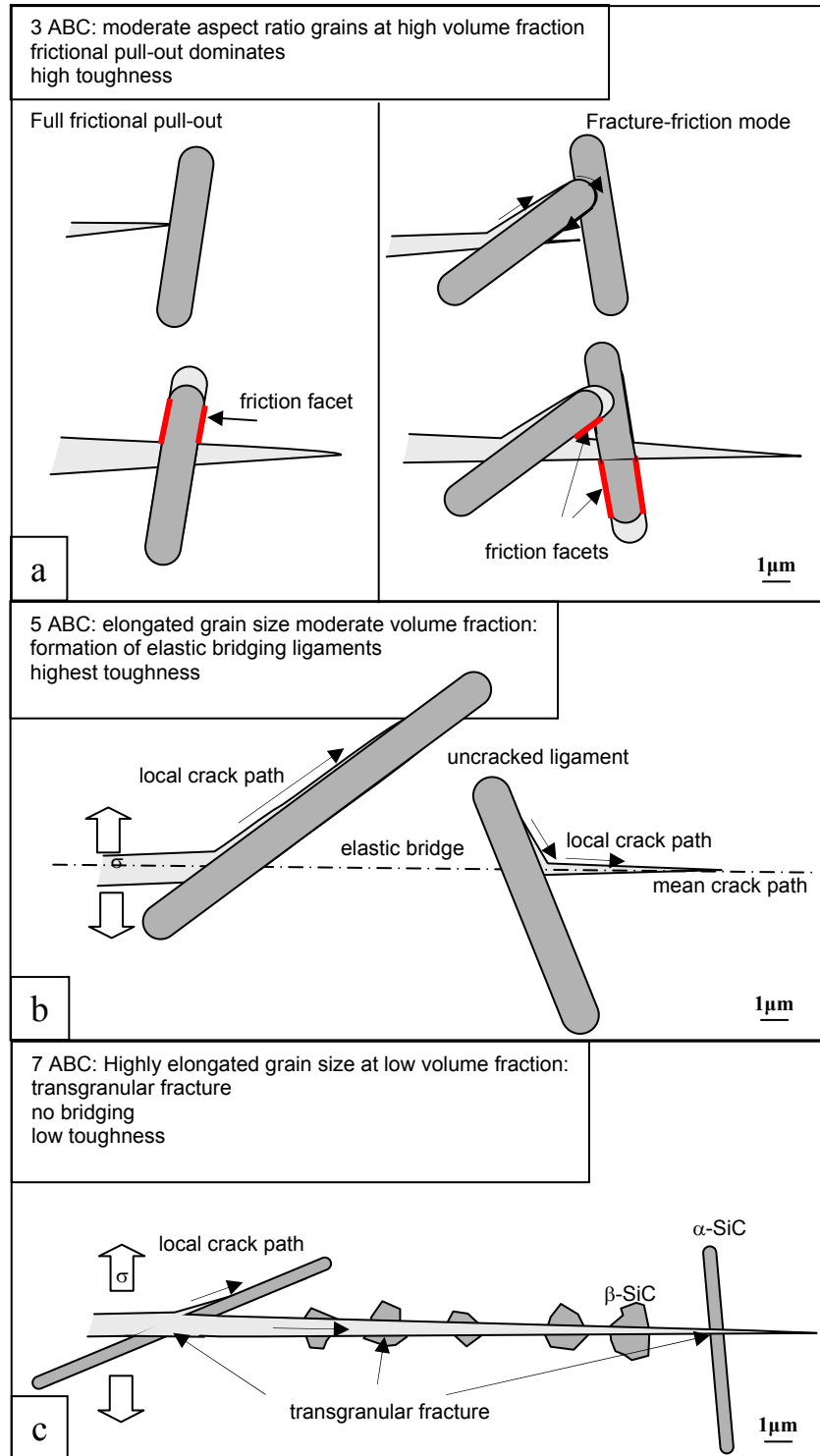transgranular fracture

1μm

c

Fig. 9. Schematic illustrations of how the crack paths lead to the development (or not) of crack bridging in (a) 3ABC, (b) 5ABC, and (c) 7ABC-SiC. Note how the predominant mode of bridging in 3ABC is from frictional grain bridging, whereas it results more from uncracked ligaments in 5ABC; in contrast, no bridging is developed in the 7ABC.

30